



1 **Investigation of the summer 2018 European ozone air pollution episodes using**
2 **novel satellite data and modelling**

3 Richard J. Pope^{1,2}, Brian J. Kerridge^{3,4}, Martyn P. Chipperfield^{1,2}, Richard Siddans^{3,4}, Barry G. Latter^{3,4},
4 Lucy J. Ventress^{3,4}, Matilda A. Pimlott¹, Wuhu Feng^{1,5}, Edward Comyn-Platt⁶, Garry D. Hayman⁷,
5 Stephen R. Arnold¹ and Ailish M. Graham¹

6
7 1: *School of Earth and Environment, University of Leeds, Leeds, United Kingdom*

8
9 2: *National Centre for Earth Observation, University of Leeds, Leeds, United Kingdom*

10
11 3: *Remote Sensing Group, STFC Rutherford Appleton Laboratory, Chilton, United Kingdom*

12
13 4: *National Centre for Earth Observation, STFC Rutherford Appleton Laboratory, Chilton, United*
14 *Kingdom*

15
16 5: *National Centre for Atmospheric Science, University of Leeds, Leeds, United Kingdom*

17
18 6: *European Centre for Medium-Range Weather Forecasts, Reading, UK*

19
20 7: *Centre for Ecology and Hydrology, Wallingford, United Kingdom*

21

22 Submitted to *Atmospheric Chemistry and Physics*

23 Correspondence to: Richard J. Pope (r.j.pope@leeds.ac.uk)

24 **Abstract:**

25 In the summer of 2018, Europe experienced an intense heat wave which coincided with several
26 persistent large-scale ozone (O₃) pollution episodes. Novel satellite data of lower tropospheric
27 column O₃ from the Global Ozone Monitoring Experiment-2 (GOME-2) and Infrared Atmospheric
28 Sounding Interferometer (IASI) on the MetOp satellite showed substantial enhancements in 2018
29 relative to other years since 2012. Surface observations also showed ozone enhancements across
30 large regions of continental Europe in summer 2018 compared to 2017. Enhancements to surface
31 temperature and the O₃ precursor gases carbon monoxide and methanol in 2018 were co-retrieved
32 from MetOp observations by the same scheme. This analysis was supported by the TOMCAT
33 chemistry transport model (CTM) to investigate processes driving the observed O₃ enhancements.
34 Through several targeted sensitivity experiments we show that meteorological processes, and
35 emissions to a secondary order, were important for controlling the elevated O₃ concentrations at the
36 surface. However, mid-tropospheric (~500 hPa) O₃ enhancements were dominated by
37 meteorological processes. We find that contributions from stratospheric O₃ intrusions ranged
38 between 15 - 40%. Analysis of back trajectories indicates that the import of O₃-enriched air masses
39 into Europe originated over the North Atlantic substantially increasing O₃ in the 500 hPa layer during
40 summer 2018.

41

42



43 1. Introduction

44 Over the past two decades there have been several intense summer-time heatwaves over Europe
45 (e.g. 2003 over continental Europe (Scott et al., 2004), 2006 over north-western Europe (Rebetez et
46 al., 2008) and 2010 across eastern Europe and Russia (Matsueda et al., 2011)). With current and
47 future climate change, increasing average global surface temperature is expected to trigger more
48 frequent and intense heatwaves (Lhotka et al., 2017; Guerreiro et al., 2018). The summer-time 2018
49 heatwave across predominantly north-western and central Europe and Scandinavia generated
50 temperature anomalies of approximately 2.0-4.0 K (Li et al., 2020; Drouard et al., 2020). Dynamically,
51 it was caused by a combination of intense anticyclonic blocking systems, Rossby wave dynamics and
52 the positive phase of the summer-time North Atlantic Oscillation (NAO+) (Li et al., 2020; Liu et al.,
53 2020; Drouard et al., 2020). Environmentally, the summer 2018 heatwave caused severe drought
54 conditions with decreased precipitation and soil moisture content (Bastos et al., 2020; Dirmeyer et
55 al., 2020), while negatively impacting natural vegetation (e.g. decreased gross primary productivity
56 (Smith et al., 2020; Bastos et al., 2020)). From a human health perspective, the 2018 heatwave
57 caused 863 temperature related excess deaths in the UK (PHE, 2019).

58 As well as dynamical and vegetation responses, enhancements in atmospheric pollutants from
59 heatwaves can lead to a degradation in air quality (AQ). Firstly, anticyclonic conditions (i.e.
60 atmospheric blocking) have been shown to cause the accumulation of primary air pollutants such as
61 carbon monoxide (CO; Thomas and Devasthale, 2014), nitrogen dioxide (NO₂; Pope et al., 2014) and
62 particulate matter (i.e. PM_{2.5}; Graham et al., 2020) to hazardous levels. Secondly, higher
63 temperatures during blocking events, which can trap and accumulate existing pollutants (e.g. Pope
64 et al., 2016), can lead to the secondary formation of tropospheric ozone (O₃). Elevated surface O₃ is
65 associated with adverse health impacts (Doherty et al., 2017; Jerrett et al., 2009) with ailments such
66 as asthma, reduced lung function and disease (WHO, 2021). It also has adverse impacts on the
67 natural biosphere (Sitch et al., 2007) and agriculture (Hollaway et al., 2012; van Dingenen et al.,
68 2009).

69 In this study, we use surface and satellite observations of O₃, in combination with the well-evaluated
70 TOMCAT global chemical transport model (CTM), to investigate the impact of the summer 2018
71 heatwave on European AQ and determine the key processes driving observed surface/tropospheric
72 O₃ enhancements. We describe the observations and model we have used in Section 2. Section 3
73 and Section 4 discusses our results and discussion/conclusions, respectively.

74 2. Observations and Model

75 2.1. Satellite and Surface Observations

76 We use satellite observations of lower tropospheric O₃ (i.e. sub-column O₃ (SCO₃) between the
77 surface and 450 hPa) from the Global Ozone Monitoring Experiment (GOME-2) and the Infrared
78 Atmospheric Sounding Interferometer (IASI) instruments on-board ESA's MetOp-A satellite, which
79 was launched in 2006 into a sun-synchronous polar orbit with equator crossing times of 9:30 (day)
80 and 21:30 (night). GOME-2 is a nadir-viewing spectrometer with spectral coverage in the ultraviolet-
81 visible (UV-Vis) of 240–790 nm (Riese et al., 2012) and a ground footprint of 40 km × 80 km in the
82 first part of the mission and 40 km × 40 km from 2013 (once Metop-B was commissioned). IASI is a
83 Michelson interferometer which observes the infrared spectral range 645 to 2760 cm⁻¹ with spectral
84 sampling of 0.25 cm⁻¹ (Illingworth et al., 2011). It measures simultaneously in four fields of view



85 (circular at nadir with a diameter of 12 km) which are scanned across track to sample a 2200 km-
86 wide swath (Clerbaux et al., 2009).

87 For GOME-2, the Rutherford Appleton Laboratory (RAL) scheme uses an optimal estimation
88 algorithm (Rodgers, 2000) to retrieve ozone height-resolved ozone distributions spanning the
89 stratosphere and troposphere (Miles et al., 2015). The scheme applied to GOME-2 has been
90 developed from that used first for GOME-1 on-board ERS-2 (Munro et al., 1998; Forster et al., 2007).
91 This is a multi-step scheme in which profile information is first retrieved in the stratosphere by
92 exploiting wavelength-dependent absorption in the O₃ Hartley band (270-307nm) and is then
93 extended into the troposphere by exploiting temperature-dependent spectral structure in the O₃
94 Huggins bands (325-335nm). For IASI, O₃ profiles are retrieved using an extended version of RAL's
95 Infrared-Microwave-Sounding (IMS) scheme, which is described in Pope et al., (2021) and Palmer et
96 al., (2022). The IMS core scheme was originally developed to retrieve temperature, water vapour
97 and stratospheric O₃ profiles along with surface spectral emissivity and cloud jointly from co-located
98 measurements by IASI, the Microwave Humidity Sounder (MHS) and the Advanced Microwave
99 Sounding Unit (AMSU-A) on MetOp (RAL Space, 2015). GOME-2 O₃ data were filtered for a geometric
100 cloud fraction less than 0.2, a solar zenith angle less than 80°, a cost function less than 200.0 and a
101 convergence flag equal to 1.0. IASI data were filtered for a geometric cloud fraction less than 0.2 and
102 a cost function less than 1000.0.

103 We also use surface O₃ observations from the European Monitoring and Evaluation Programme
104 (EMEP) network for May-August 2017 and 2018. In total, we used 83 spatial collocated EMEP sites in
105 both years across Europe. Here, data at individual sites were selected where the
106 corresponding data flag was set to 0.0.

107 2.2. Modelling & Sensitivity Experiments

108 In this study the TOMCAT CTM (Chipperfield, 2006) is forced by European Centre for Medium-Range
109 Weather Forecasts (ECMWF) ERA-Interim reanalysis meteorology (Dee et al., 2011) and run at a
110 horizontal resolution of 2.8° × 2.8° with 31 vertical levels from the surface to 10 hPa. The model
111 includes detailed tropospheric chemistry, including 229 gas-phase reactions and 82 advected tracers
112 (Monks et al., 2017), and heterogeneous chemistry driven by size-resolved aerosol from the
113 GLOMAP module (Mann et al., 2010). Simulations used here include year-specific anthropogenic
114 emissions from MACCity (Granier et al., 2011) and fire emissions from the Global Fire Assimilation
115 System (GFAS, Kaiser et al., 2012). Year-specific off-line biogenic volatile organic compounds (VOCs)
116 emissions for acetone, methanol, isoprene and monoterpenes were simulated by the Joint UK Land
117 Environment Simulator (JULES – Pacifico et al., 2011; Best et al., 2011; Clark et al., 2011). All other
118 biogenic VOC emissions are climatological values and provided by the Chemistry-Climate Model
119 Initiative (CCMI) (Morgenstern et al., 2017). The global budgets of the JULES VOC emissions are low
120 in comparison to the climatological CCMI emissions, so were scaled up on a regional basis, while
121 retaining the 2017-2018 step change related to the 2018 summer heat wave. The full details of
122 JULES VOC emissions scaling can be found in **Supplementary Material (SM) 3**. The model was run for
123 2017 and 2018 with output at 6-hourly intervals (i.e. 00, 06, 12 and 18 UTC). Here, each year was run
124 with its respective meteorology and emissions and given the labels Met17_Emis17 (representing
125 2017) and Met18_Emis18 (representing 2018).

126 To explore the importance of emission and meteorological processes behind the elevated European
127 summer 2018 tropospheric O₃ levels, a 1-year model sensitivity experiment was performed using



128 2018 meteorology but 2017 emissions (i.e. Met18_Emis17). Therefore, the difference between
129 Met18_Emis17 and Met17_Emis17 highlights the impact of fixed emissions (i.e. 2017 emissions for
130 both years), while the Met18_Emis18 minus Met18_Emis17 highlights the impact of fixed
131 meteorology (i.e. 2018 meteorology for both years). These are compared with the control
132 differences for 2018-2017 (Met18_Emis18- Met17_Emis17). From here on in, we refer to the control
133 differences, fixed emission differences and the fixed meteorology differences as CTL_DIFF,
134 FIXED_EMIS_DIFF and FIXED_MET_DIFF, respectively. TOMCAT also includes a stratospheric O₃
135 tracer (i.e. tags O₃ in the model which originated in the stratosphere). This was used to investigate
136 the impact of stratospheric O₃ intrusion into the troposphere.

137 TOMCAT has been used in a number of previous studies to investigate air quality and tropospheric
138 composition (e.g. Richards et al., 2013; Emmons et al., 2015; Pope et al., 2016; Pope 2020) whose
139 results give confidence in the model's ability to simulate European tropospheric O₃ in this study.
140 Overall, when compared with observations, TOMCAT has good spatial agreement with both GOME-2
141 and IASI and can reasonably reproduce the 2018 SCO₃ enhancement in 2018 versus 2017 (SM 4). The
142 model also has good agreement, both in magnitude and seasonality, with the EMEP observed
143 surface concentrations (SM 4).

144 2.3 ROTRAJ Back-trajectories

145 We use the Reading Offline Trajectory Model (ROTRAJ) to generate air mass back-trajectories
146 (Methven et al., 2003) to assess the import of tropospheric O₃ into Europe. ROTRAJ is a Lagrangian
147 atmospheric transport model driven by meteorology from the same ECMWF ERA-Interim reanalyses
148 as used by TOMCAT. Velocity fields at the Lagrangian particle positions are determined by cubic
149 Lagrange interpolation in the vertical, bilinear interpolation in the horizontal and linear interpolation
150 in time. Kinematic back-trajectories were released at 6-hourly intervals (i.e. at 00, 06, 12 and 18 UTC)
151 from Paris and Berlin, both central locations over Europe in the region of summer-time 2018 O₃
152 enhancements, between the 1st May and 31st August for both 2017 and 2018. The trajectories were
153 released at the surface and at approximately 500 hPa and integrated for 10 days with 6-hourly
154 output (i.e. 41 trajectory points including the starting location) to investigate the origin of air masses
155 arriving in these altitude regions of enhanced summer-time O₃ in 2018. In total, ROTRAJ was
156 therefore run 8 times (2 years × 2 altitudes × 2 locations).

157 To quantify the import of tropospheric O₃ into Europe, for each trajectory, all the trajectory points
158 were co-located with corresponding TOMCAT O₃ mixing ratio values (i.e. the horizontal and vertical
159 grid box the trajectory point sits within and corresponding time stamp) and then the average O₃-
160 weighted back-trajectory (O₃-WBT) determined (i.e. back-trajectories with larger O₃WBT values
161 come from air masses with larger O₃ content).

162 3. Results

163 3.1 Surface Temperature

164 Several studies (e.g. Li et al., 2020; Liu et al., 2020; Drouard et al., 2020) have documented the
165 intense heat wave across Europe in the summer of 2018. This is further shown in Figure 1 which
166 compares surface temperature, co-retrieved with ozone and other variables from MetOp-A by the
167 IMS scheme, between 2017 and 2018. In May, higher temperatures occur across Scandinavia (5.0-
168 10.0 K), eastern Europe (3.0-7.0 K) and the UK (1.0-3.0 K), but temperatures are lower (-3.0 to -1.0 K)
169 across Iberia. In June, a similar spatial distribution occurs but the magnitude of the differences is



170 smaller. In July the largest temperature increases range from 6.0-8.0 K in Scandinavia to 2.0-6.0 K in
171 the UK/France. Iberia continued to experience temperatures lower by -2.0 to 0.0 K. In August, there
172 are near-zero differences over the UK, Iberia and most of Scandinavia but with increases of 1.0-3.0 K
173 over eastern Europe and Finland.

174

175 3.2 Satellite Ozone

176 We investigate the longer term variability in tropospheric O₃ (i.e. SCO₃) to determine if 2017 is a
177 suitable comparator for the 2018 summer O₃ enhancements as it is for temperature. **Figure 2** shows
178 the 2012-18 SCO₃ average between May and August for a domain over the Atlantic and Europe and
179 the difference for the same season between specific years and the 2012-18 average. In 2012 and
180 2013, there are significant positive differences from the average between 1.0 DU and 5.0 DU over
181 much of the domain. Over continental Europe, the differences are smaller. Here, the significance of
182 differences between the year-specific and long-term averages are determined using the Wilcoxon
183 Rank test (Pirovano et al., 2012) at the 95% confidence level. In 2014 and 2015, there are negative
184 differences across Europe (-4.0 DU to -1.0 DU). In 2016, similar negative differences are primarily
185 across the north and south-east of the domain. In 2017, there are near-zero differences across the
186 Atlantic, UK and western Europe. Over eastern Europe and Mediterranean, there are significant
187 negative differences of between -2.0 DU and -1.0 DU. In 2018, across continental Europe there are
188 significant positive differences between 2.0 DU and 4.0 DU. As the 2017 differences are relatively
189 small in magnitude with a low proportion of significant pixels (i.e. Sig Pixels % = 32.7 is the lowest
190 across the 7 years), it is representative of average conditions for comparison with 2018. For 2018,
191 the summer SCO₃ enhancements across continental Europe are the largest for the years shown with
192 a coherent cluster of significant differences. This illustrates that the summer 2018 SCO₃
193 enhancements are a substantial deviation from the average conditions (which we represent as 2017
194 hereon) and that this is an intense O₃ event.

195 Investigation of SCO₃ retrieved from both GOME-2 (**Figure 3**) and the IMS scheme (**Figure 4**) show
196 consistent enhancements in summer 2018. In 2017, between May and August, GOME-2 typically
197 observed SCO₃ values between 20.0-30.0 DU across continental Europe. Peak SCO₃ values occurred
198 over the Mediterranean (30.0-38.0 DU); relatively high ozone is a typical feature of the
199 Mediterranean in summer (Richards et al., 2013). In 2018, the seasonality is consistent with 2017,
200 but the continental European SCO₃ values ranged between 25.0 DU and 35.0 DU. For the 2018-2017
201 difference, SCO₃ enhancements occur across continental Europe in all four months, but peaked in
202 May and July between 3.0 DU and 8.0 DU, while typically 1.0-5.0 DU in June and August. The spatial
203 distribution of IMS-retrieved SCO₃ is similar to that of GOME-2 in 2017 and 2018, although the
204 absolute values tend to be systematically lower by 3.0-4.0 DU. However, despite this systematic
205 offset, the 2018-2017 differences are reasonably consistent with GOME-2. Across continental
206 Europe, IMS SCO₃ shows 2018 enhancements in all months investigated, but peaks in May and July,
207 like GOME-2, between 3.0 DU and 6.0 DU. The differences range from 1.0 DU to 3.0 DU in June and
208 are approximately 1.0 DU in August (though a peak enhancement of 3.0-5.0 DU occurs over the
209 Mediterranean). Spatial correlations between the GOME-2 and IASI difference (i.e. 2018-2017) maps
210 for the months investigated ranged between 0.21 and 0.47 (see **SM 4**).

211 The GOME-2 and IASI instruments observe UV-Vis and IR wavelengths, with peak vertical sensitivities
212 to tropospheric O₃ in the lower and mid/upper troposphere, respectively. Consistency in the 2018



213 enhancements in SCO_3 indicates that these extend over the bulk of the troposphere and increases
214 confidence in the differences for both sensors.

215 Investigation of several satellite-retrieved O_3 precursor gases (see **SM 1**) showed enhancements in
216 total column methanol (TCCH_3OH , **Figure S1**), especially linked to May and July temperature
217 enhancements (**Figure 1**), minor increases in tropospheric column NO_2 (TCNO_2 , **Figure S2**) in May and
218 July over central Europe and widespread enhancements (weakest in July and strongest in August) in
219 total column carbon monoxide (TCCO , **Figure S3**). Investigation of the GOME-2 and IASI total column
220 O_3 (TCO_3) differences between 2017 and 2018 (**Figures S4 & S5**) showed these to be in close
221 agreement. Some spatial structure is similar to that of the SCO_3 difference patterns (**Figures 3 and**
222 **4**), with correlations of approximately 0.5 between TCO_3 and SCO_3 for each instrument (see **SM 2**).
223 Given the complex relationship between tropospheric O_3 , precursor gases, atmospheric chemistry
224 (e.g. NO_x or VOC-limited regimes), surface deposition and meteorological conditions (e.g.
225 atmospheric temperatures and transport), a detailed chemistry transport model is required to assess
226 the key processes leading to the observed SCO_3 enhancements over Europe.

227 3.3 Surface Ozone

228 Increased temperatures during heat waves have been shown to enhance surface O_3 concentrations
229 (e.g. Jacob and Daniel, 2009; Vieno et al., 2010; Pyrgou et al., 2018). In the summer (May-June-July-
230 August, MJJA) of 2018, EMEP recorded larger O_3 mixing ratios across most of Europe in comparisons
231 to 2017 (**Figure 5a & b**). Over central Europe, surface O_3 mixing ratios ranged from approximately
232 45.0 ppbv to over 60.0 ppbv, while in 2017 it was 35.0 ppbv to 50.0 ppbv. Over the UK and north-
233 western Europe, surface O_3 mixing ratios ranged from 20.0 ppbv to 30.0 ppbv and then 25.0 ppbv to
234 35.0 ppbv in MJJA 2017 and 2018, respectively. In Scandinavia and eastern Europe, surface O_3 mixing
235 ratios ranged from 20.0 ppbv to 35.0 ppbv in MJJA 2017, while increasing to 25.0 ppbv to
236 approximately 40.0 ppbv in MJJA 2018. **Figure 5c** highlights these widespread enhancements where
237 domain-average surface O_3 mixing ratios are larger by typically 5.0-10.0 ppbv in May and from mid-
238 June to mid-August in 2018. **Figure 5d** shows that the domain median surface O_3 concentration
239 across MJJA was larger by 2.0-3.0 ppbv, but the 2018 extremes were greater with 75th and 95th
240 percentiles of 42.0 ppbv and 53.0 ppbv in 2017 and 47.0 ppbv and 59.0 ppbv in 2018. Therefore,
241 surface observations of O_3 recorded widespread enhancements in MJJA 2018 compared to 2017
242 with peak site differences >10.0 ppbv. This is generally consistent with the 2018 layer-averaged
243 enhancements in the satellite-retrieved SCO_3 for regions where both datasets have spatial coverage.

244 3.4. Model Simulations

245 We use the TOMCAT model to investigate different factors potentially driving the observed
246 enhancements in tropospheric O_3 . In comparisons with the observations (see **SM 4**) the model
247 reproduces the sign and spatial distribution of observed 2018-2017 differences reasonably well.
248 Although it has a tendency to underestimate the absolute magnitude, we are confident in the
249 model's ability to simulate the tropospheric O_3 enhancements relative to 2017.

250 At the surface (**Figure 6**), TOMCAT CTL_DIFF (i.e. Met18_Emis18 - Met17_Emis17) suggests that O_3 is
251 enhanced in May over Scandinavia (2.0- >5.0 ppbv), north-western Europe (0.0-2.0 ppbv), the Arctic
252 Ocean (>5.0 ppbv) and off the coast of Iberia (3.0-5.0 ppbv). However, negative values exist over
253 eastern Europe (-3.0 ppbv to -1.0 ppb) and the Atlantic west of Ireland (-3.0 ppbv to -1.0 ppb). In
254 June, the negative differences persist in eastern Europe (-3.0 ppbv to -1.0 ppb), but positive



255 differences are located over northern Scandinavia (1.0-2.0 ppbv) and the North Atlantic (2.0-4.0
256 ppbv). For July, CTL_DIFF shows the largest enhancements over continental Europe (i.e. Po Valley,
257 France, Benelux region and Iberia) and the UK (>5.0 ppbv). Negative differences of between -3.0
258 ppbv and -1.0 ppbv remain over eastern Europe. In August, the only clear differences are over Iberia
259 and the western Mediterranean, ranging between 3.0 ppbv and >5.0 ppbv. Overall, TOMCAT
260 simulates sub-regional surface O₃ enhancements over Europe, which are generally consistent with
261 EMEP observations apart from several sites over eastern Europe.

262 At 500 hPa, TOMCAT CTL_DIFF shows larger-scale O₃ enhancements in 2018 compared to 2017 (>5.0
263 ppbv) throughout May to August. In May and August, there are, however, a few negative differences
264 (-5.0 ppbv to -3.0 ppbv) over far eastern Europe. In June and July, the full domain is more or less
265 dominated by O₃ enhancements in 2018. In Figures 4 and 5 (and SM 4), GOME-2 and IASI (and
266 TOMCAT with the instrument averaging kernels (AKs) applied to account for the vertical sensitivity of
267 the retrievals, see SM 4 for more information) show SCO₃ enhancements during these months of
268 2018. Given the vertical extents and peak heights of their retrieval sensitivities and consistency in
269 spatial patterns (Figs SM-8 and 10) it is evident that the O₃ enhancements detected by GOME-2 and
270 IASI extend over the free troposphere. The model shows large-scale O₃ enhancements in the free
271 troposphere and similar patterns to GOME-2 and IASI when averaging kernels applied. So the model
272 corroborates this finding from the satellite retrievals. Signals from EMEP and TOMCAT at the surface,
273 on the other hand, are more mixed across the domain.

274 The right-hand column of Figure 6 shows the relative difference in the stratospheric O₃ contribution
275 to the 500 hPa O₃ layer (i.e. Strat % @ 500 hPa), from CTL_DIFF, between 2017 and 2018. Here, the
276 percentage of stratospheric O₃ contributing to the O₃ concentration at the 500 hPa is calculated for
277 2017 and 2018 and then the 2018-2017 difference determined. The largest enhancement to the 500
278 hPa layer was in July where the stratospheric O₃ contribution increased by 3.0% to >5.0% across
279 Europe. In June and August, the spatial patterns are similar with stratospheric O₃ contribution
280 enhancements of 3.0-5.0% across southern Europe, Scandinavia and the North Atlantic (above the
281 UK). In the North Atlantic, UK and northern Europe, there are near-zero changes in June and August.
282 In May, there are enhancements >5.0% across the northern region of the domain and northern
283 Africa, while smaller enhancements (1.0%-3.0%) over the UK and near-zero changes over eastern
284 Europe. This is partially supported by analysis of TCO₃ (see SM 2) where there are reasonable spatial
285 correlations (~0.5 to 0.6) between the SCO₃ 2017-2018 summer differences and the equivalent for
286 TCO₃. Therefore, these results indicate a potentially enhanced contribution of stratospheric O₃ into
287 the mid-troposphere during the summer of 2018 across Europe.

288 To quantify the separate importance of precursor emissions and meteorology in governing the
289 summer 2018 O₃ enhancements we compare the sensitivity experiments with the control runs.
290 Figure 7 (left column) shows the results for the fixed emissions differences (i.e. FIXED_EMIS_DIFF)
291 between years (i.e. Met18_Emis17 – Met17_Emis17). At the surface, the FIXED_EMIS_DIFF show
292 similar spatial patterns to that of CTL_DIFF (Figure 6 – left column). The domain spatial difference
293 correlations between these simulations is greater than 0.96 for all months considered. However,
294 FIXED_EMIS_DIFF (Figure 7 - left column) tends to be lower than CTL_DIFF (Figure 6 – left column)
295 by approximately 0.0-2.9 ppbv (i.e. positive red regions are weaker and negative blue regions
296 stronger in intensity). Therefore, the Met18_Emis17 run struggles to reproduce the absolute surface
297 O₃ enhancements in the Met18_Emis18 run. When the fixed meteorology differences



298 (FIXED_MET_DIFF, i.e. Met18_Emis18 - Met18_Emis17, **Figure 8** - left column) are compared with
299 CTL_DIFF, the surface 2018-2017 differences are substantially different.

300 Surface FIXED_MET_DIFF ranges between 0.0 ppbv and 2.0 ppbv across the domain in May and June
301 and is more confined to continental Europe in July and August. This shows that TOMCAT simulates
302 lower 2018 summer-time O₃ when 2017 emissions are used and indicates that emissions do have
303 some role in controlling O₃ levels at the surface. However, as the spatial difference pattern for
304 FIXED_MET_DIFF (**Figure 8** – left column) is different to that of CTL_DIFF (**Figure 6** – left column),
305 spatial correlations between them range from -0.53 to 0.54 over the four months, it suggests that
306 meteorology is important in governing the spatial distribution of CTL_DIFF. This is supported by the
307 fact that FIXED_MET_DIFF - CTL_DIFF (**Figure 8** left column – **Figure 6** left column) yields absolute
308 domain variations between 0.0 ppbv and 12.2 ppbv. Therefore, the two sensitivity experiments
309 suggest meteorology and emissions both play important roles in controlling surface O₃ during the
310 summer of 2018, but meteorology predominantly governs the spatial pattern and absolute
311 magnitude of the O₃ enhancements.

312 At 500 hPa, comparison of FIXED_EMIS_DIFF and CTL_DIFF show very consistent spatial patterns
313 across the four months with correlations all above 0.98. In terms of the absolute differences
314 between FIXED_EMIS_DIFF and CTL_DIFF (i.e. **Figure 7** centre column – **Figure 6** centre column) it
315 peaks at approximately 2.8 ppbv. For FIXED_MET_DIFF, the spatial correlation with CTL_DIFF, as for
316 the surface, is variable with values between -0.38 and 0.43. The absolute differences between
317 FIXED_MET_DIFF and CTL_DIFF (i.e. **Figure 8** centre column – **Figure 6** centre column) ranges from
318 0.0 ppbv to 14.8 ppbv. Therefore, emissions have a secondary role in controlling the O₃ while
319 meteorology is by far the dominant factor. For Strat % @ 500 hPa, the spatial correlations between
320 CTL_DIFF and FIXED_EMIS_DIFF are above 0.95 for all months and the absolute differences between
321 them (i.e. **Figure 7** right column - **Figure 6** right column) are near-zero. Comparison of
322 FIXED_MET_DIFF and TC_CTL shows spatial difference correlations ranging between -0.33 and 0.71
323 and absolute differences (i.e. **Figure 8** right column - **Figure 6** right column) peaking at 12.9%.
324 Therefore, as expected, meteorological processes are dominating the influence of the stratospheric
325 O₃ contribution (i.e. through stratosphere-troposphere exchanges) to the 500 hPa layer during the
326 summer 2018 O₃ enhancements over Europe.

327 To investigate the importance of stratospheric-troposphere exchange to the middle troposphere
328 enhancement (i.e. as shown in the TOMCAT 500 hPa layer and the satellite SCO₃ data), **Figures 9** and
329 **10** show TOMCAT control run zonal 2018-2017 difference cross-sections (for the domain longitudes)
330 of O₃ profiles and the stratospheric O₃ contribution to each pressure layer. In May and June, in the
331 lower troposphere (approximately surface to 800 hPa), there are negative (-3.0% to 0.0%) and
332 positive (0.0% to 3.0%) differences between 30-50°N and 50-70°N, respectively. During June, there
333 are positive differences (0.0% to 5.0%) across most latitudes and in August, the opposite occurs to
334 that of May/June. In the mid-troposphere (800-300 hPa), positive differences occur in most months
335 (0.0-5.0% in May, 0.0-7.0% in June, >10% in July and 5.0-10.0% in August), though in May and August
336 negative differences (-5.0% to 0.0%) exist around 40°N and 55°N. This is consistent with the 500 hPa
337 O₃ differences in **Figure 6** (centre panels). In the upper troposphere – lower stratosphere (UTLS,
338 approximately 300-100 hPa) there are limbs of positive O₃ differences (i.e. >10%, 5.0-10.0 ppbv)
339 propagating into the mid-troposphere (30-40°N in May, 30-50°N in June, 40-50°N in July and 30-40°N
340 & 60-70°N in August), suggestive of stratospheric intrusion into the mid-troposphere. Using the
341 stratospheric O₃ tracer in TOMCAT, **Figure 10** shows the enhanced proportion of O₃ originating from



342 the stratosphere in the summer of 2018. Interestingly, for all months (apart from May between 30-
343 45°N), there are enhanced contributions of stratospheric O₃ (15.0% to >50.0%) in the lower-mid
344 troposphere (i.e. below 500 hPa). In absolute terms, this is only a minor contribution typically below
345 800 of <1.0 ppbv. Between 800-400 hPa, this increases to 1.0-5.0 ppbv (remains relatively consistent
346 in percentage terms) in most months and latitude bands. In the UTLS, it increases to 5.0-10.0%
347 enhancements in stratospheric O₃ contributions, which is consistent with its proximity to the
348 stratosphere. In comparison between **Figures 9** and **10**, where there are enhancements in the
349 stratospheric O₃ contribution but negative differences in O₃ (e.g. in June in the lower troposphere
350 between 50°N and 55°N) which is suggestive of different processes influencing the O₃ concentrations
351 (e.g. descent of relatively small stratospheric O₃ contributions but advection of tropospheric O₃ away
352 from the region). Overall though, in the mid-troposphere, where there are larger enhancements in
353 O₃, there are similar responses in the stratospheric O₃ contribution. For June, the mid-troposphere
354 O₃ enhancement is approximately 5.0-7.0 ppbv with a signal of 1.0-2.0 ppbv in the stratospheric
355 tracer. Therefore, in the more extreme cases, the stratospheric O₃ contribution is approximately
356 15.0-40.0% to the mid-tropospheric O₃ enhancements in summer 2018 over Europe.

357 The two remaining factors, linked to meteorological processes (as suggested above), which may
358 affect the O₃ enhancements in 2018 are increased summer temperatures (e.g. through enhanced
359 kinetic rates), and the import of tropospheric O₃ from upwind (e.g. North America from the
360 prevailing winds). **Figure 11** shows the 2017-2018 zonal temperature differences (i.e. same as **Figure**
361 **9** but for temperature) with the correlation between the 2017 and 2018 temperature and O₃
362 differences overplotted. Qualitatively, the zonal differences in O₃ and temperature have some
363 similarities. There are positive differences (temperature differences of 0.0-1.0%) between 50-60°N
364 and the surface and 400 hPa in May and June. Then in July, collocated positive differences (peaking
365 at 2.0% or 3.0 K) exist between 50-70°N from the surface to 300 hPa. In August, there is no clear
366 relationship between temperature and O₃ enhancements. In all months (to a lesser extent in
367 August), in the UTLS, there are spatial agreements with positive differences between approximately
368 30-45°N and negative differences between 50/55-70°N. In terms of correlations (i.e. temporal
369 correlation in each grid box using the TOMCAT 6-hourly time series), the spatial agreement is
370 relatively weak. In all months, most of domain has relatively small values ranging between -0.5 to
371 0.5. There are only a few locations with strong correlations (i.e. > 0.5), which are in the UTLS or in
372 the lower-mid troposphere between 50-70°N (June & August) and 45-55°N in July near the surface.
373 Overall, the relationship between increased temperatures and enhanced kinetic rates yielding more
374 ozone formation is non-linear, so it is unsurprising that the direct comparisons of temperature and
375 ozone 2018-2017 differences above shows no clear pattern. Therefore, future work could include a
376 further sensitivity experiment running TOMCAT for 2018, but with 2017 temperatures used in the
377 chemistry routines to quantify the role of temperature in the summer 2018 O₃ enhancements.

378 To investigate the potential advection of tropospheric O₃-rich air masses into Europe we have used
379 ROTRAJ back-trajectories to determine the O₃WBTs (i.e. an indicator of air mass O₃ content). As
380 shown in **SM 5**, there is large variability in the O₃WBT values and spatial distribution (i.e. **Figures SM**
381 **12** and **13**), so they have to be gridded onto the TOMCAT horizontal resolution (see **Figures SM14**
382 and **15**). **Figure 12** shows the differences (2018-2017) between the gridded O₃WBTs where the back-
383 trajectories have been released at the surface from Paris (**Figure 12a**), at the surface from Berlin
384 (**Figure 12b**), at approximately 500 hPa from Paris (**Figure 12c**) and at approximately 500 hPa from
385 Berlin (**Figure 12d**). We selected Paris and Berlin as they are situated in central Europe where the



386 summer 2018 O₃ enhancements have been observed while the surface and 500 hPa are the altitudes
387 of primary focus in the modelling work.

388 At the surface, Paris and Berlin show consistent patterns. Over the North Atlantic (i.e. origin of the
389 prevailing winds into Europe), there are typically negative O₃WBT values between -5.0 ppbv and -1.0
390 ppbv suggesting that advection of O₃ into Europe during the summer (i.e. May-August) was
391 predominantly larger in 2017 and did not strongly contribute to the 2018 observed surface O₃
392 enhancements. Advection of O₃-rich air in 2018 did originate from Scandinavia into continental
393 Europe, though the number of trajectories is relative low (see **Figure S12**). As both locations show
394 similar relationships, it provides confidence in this methodology. At 500 hPa, the 50-60°N spatial
395 pattern is less defined with values typically between -5.0 and 5.0 ppbv for both locations. However,
396 in the southern North Atlantic (30-50°N) there are positive differences of approximately 3.0-10.0
397 ppbv for both release locations. Note that as free-tropospheric winds tend to have larger horizontal
398 velocities, the back-trajectories generally start from further away closer to North America. Again,
399 given the broad similarity in differences between both release locations, it provides confidence in
400 this approach. Overall, our results indicate a larger transport of O₃ to the surface of continental
401 Europe in 2017, while at approximately 500 hPa the import of O₃ into Europe is larger in 2018. Here,
402 the positive differences originate from the southern North Atlantic (i.e. a larger range of locations,
403 absolute values and homogeneous signal than the mixed differences between 50-60°N).

404 One potentially important factor is dry deposition of O₃ to the land surface. Due to the heatwave,
405 stress on the biosphere and the associated die back of vegetation could potentially reduce the
406 efficiency of O₃ deposition decreasing the O₃ sink (i.e. O₃ is more likely to deposit onto land covered
407 by vegetation than bare soil). Investigation of the normalised difference vegetation index (NDVI),
408 from the IMS scheme, between the summers of 2017 and 2018 did not highlight any spatially
409 coherent changes (not shown here). As a result, there is no obvious large-scale spatial vegetation die
410 back in 2018 due to the heatwave and thus the impact this would have on ozone deposition in
411 TOMCAT. Therefore, we ran two further experiments where the bare soil fraction for each grid box
412 over Europe was increased and decreased by 25% in summer 2018. This was to investigate the
413 sensitivity of surface ozone deposition to changes in the land surface. For the increase in bare soil
414 fraction there was a moderate systematic increase in European summer ozone by 0.0-1.5 ppbv (i.e.
415 less ozone deposition). When the bare soil fraction was decreased by 25%, this yielded a small
416 decrease in surface ozone by approximately 0.5 ppbv. Overall, a sizable level of vegetation die back
417 would be required for decreased ozone dry deposition to substantially contribute to the summer
418 2018 surface ozone enhancements.

419 **4. Discussion and Conclusions**

420 The summer of 2018 produced an intense heatwave across most of Europe with a substantial impact
421 on tropospheric temperatures, droughts, stress on vegetation and human mortality. Observations of
422 surface temperature, precursor gases and total column O₃ (TCO₃) experienced enhancements in
423 2018 relative to 2017. In this paper we have demonstrated a strong enhancement in surface and
424 tropospheric O₃ during the heatwave between May and August 2018. The EMEP surface data
425 suggest an average European enhancement, relative to 2017, peaking at approximately 10.0 ppbv in
426 July and August. Investigation of lower tropospheric O₃ (i.e. surface-450 hPa sub-column O₃ – SCO₃)
427 from the GOME-2 and IASI instruments also showed enhancements, peaking at 5.0-10.0 DU, relative
428 to 2017. Analysis of the long-term GOME-2 SCO₃ record indicates 2017 to be a suitably



429 neutral/average reference year and the enhancement in 2018 to be anomalously large. Our
430 comparisons were therefore made between the summers of 2017 and 2018.

431 Consistency between the UV (GOME-2) and IR (IASI) sounders was important to our analysis because
432 their vertical sensitivities peak in the lower and mid-upper troposphere, respectively. The similar
433 patterns of SCO_3 enhancement detected by the two sounders therefore indicate that these extend
434 over the bulk of the troposphere, supportive of surface/lower tropospheric ozone enhancements.
435 This consistency also provides confidence that the complementary vertical sensitivities of GOME-2
436 and IASI ozone retrievals could be exploited in further investigation of tropospheric ozone (e.g. long-
437 term trends from multiple platforms/retrieval schemes has shown large-scale inconsistencies in
438 other studies e.g. Gaudel et al., (2018)) in the future.

439 Tropospheric O_3 behaviour is complex and the summer 2018 enhancements over Europe could
440 potentially have been caused by various factors: atmospheric chemistry, meteorology (e.g.
441 temperature, advection of O_3 -rich air masses), anthropogenic and natural precursor emissions, dry
442 deposition and stratospheric intrusion. To investigate the interactions between these processes,
443 potentially leading to the summer 2018 O_3 enhancements, we used the well-evaluated TOMCAT 3D
444 CTM. Evaluation of the model in this study showed that it could accurately capture the spatial
445 pattern, temporal evolution and sign (i.e. positive 2018-2017 O_3 differences) of the O_3
446 enhancements and that, although it underestimated the observed enhancements, TOMCAT is an
447 adequate tool to investigate them.

448 The results of several model simulations showed that the surface ozone enhancements (mainly in
449 north-western Europe) in the summer of 2018 were predominantly driven by meteorological
450 processes with emissions acting as a secondary factor. As the ROTRAJ back-trajectories suggest that
451 advection of summer-time O_3 was larger in 2017, the 2018 European O_3 enhancements at surface
452 level were likely from in-situ processes. The TOMCAT stratospheric O_3 tracer indicated a negligible
453 contribution of stratospheric O_3 to these surface enhancements. At 500 hPa, the enhancement in
454 tropospheric O_3 is much larger spatially across Europe and dominated by meteorological processes.
455 Intrusion of stratospheric O_3 into the mid-troposphere has a moderate influence on the
456 observed/modelled O_3 enhancements with contributions of up to 15.0-40.0%. Correlations between
457 TOMCAT temperature and O_3 enhancements show broad agreement at some latitudes (e.g. 50-70°N
458 in the lower-mid troposphere). However this relationship is non-linear and difficult to quantify
459 without further simulations/model tracers, which was beyond the scope of this study. ROTRAJ back-
460 trajectories suggest that in 2018, relative to 2017, there is the advection of more O_3 -rich airmasses
461 into the European mid-troposphere contributing to the summer 2018 O_3 enhancements at this
462 altitude. Therefore, in the summer of 2018 over Europe, in-situ meteorological processes appear to
463 be predominantly driving surface O_3 enhancements over Europe, while advection of tropospheric O_3 -
464 rich air and stratospheric intrusion are driving the corresponding tropospheric O_3 .

465 **Acknowledgements**

466 This work was funded by the UK Natural Environment Research Council (NERC) by providing funding
467 for the National Centre for Earth Observation (NCEO, award reference NE/R016518/1).

468 **Conflicting Interests**

469 The authors declare that they have no conflicts of interest.

470 **Date Availability**



471 The TOMCAT simulations are publically available at
472 http://homepages.see.leeds.ac.uk/~earrjpo/european_summer_2018_o3/tomcat, while the RAL
473 Space satellite can be found at
474 http://homepages.see.leeds.ac.uk/~earrjpo/european_summer_2018_o3/satellite. The EMEP
475 surface O₃ data was obtained from <http://ebas-data.nilu.no/default.aspx>. The GOME-2 tropospheric
476 column NO₂ data was downloaded from EUMETSAT at https://acsaf.org/nrt_access.php. The
477 TOMCAT and RAL Space satellite data will be uploaded to the Zenodo open access portal
478 (<https://zenodo.org/>) if this manuscript is accepted for publication in ACP after the peer-review
479 process.

480 Author Contributions

481 RJP, MPC and BJK conceptualised and planned the research study. RJP performed the TOMCAT
482 model simulations with support from MPC and WF. The JULES BVOC emissions were provided by ECP
483 and GDH. RJP analysed the satellite data provided by RAL Space (BJK, RS, BGL and LJV) with support
484 from BJK, RS and BGL. RJP undertook the EMEP analysis. RJP ran ROTRAJ with technical support from
485 SRA and AMG. RJP prepared the manuscript with contributions from all co-authors.

486 References

- 487 Bastos, A., Ciais, P., Friedlingstein, P., et al.: Direct and seasonal legacy effects of the 2018 heat wave
488 and drought on European ecosystem productivity, *Science Advances*, 6, eaba2724,
489 doi:10.1126/sciadv.aba2724, 2020.
- 490 Best, M.J., Pryor, M., Clark, D.B., et al.: The Joint UK Land Environment Simulator (JULES), model
491 description—Part 1: energy and water fluxes, *Geoscientific Model Development*, 4, 677–699,
492 doi:10.5194/gmd-4-677-2011, 2011.
- 493 Chipperfield, M.P.: New version of the TOMCAT/SLIMCAT off-line chemistry transport model:
494 Intercomparison of stratospheric trace experiments, *Quarterly Journal of the Royal Meteorological
495 Society*, 132, 1179–1203, doi:10.1256/qj.05.51, 2006.
- 496 Clark, D. B., Mercado, L.M., Sitch, S., et al.: The Joint UK Land Environment Simulator (JULES), model
497 description—Part 2: carbon fluxes and vegetation dynamics, *Geoscientific Model Development*, 4,
498 701–722, doi:10.5194/gmd-4-701-2011, 2011.
- 499 Clerbaux, C., Boynard, A., Clarisse, L., et al.: Monitoring of atmospheric composition using the
500 thermal infrared IASI/MetOp sounder, *Atmospheric Chemistry and Physics*, 9 (16), 6041–6054,
501 doi:10.5194/acp-9-6041-2009, 2009.
- 502 Dee, D.P., Uppala, S.M., Simmons, A.J., et al.: The ERA-Interim reanalysis: Configuration and
503 performance of the data assimilation system, *Quarterly Journal of the Royal Meteorological Society*,
504 137 (656), 553–597, doi:10.1002/qj.828, 2011.
- 505 Dirmeyer, P.A., Balsamo, G., Blyth, E.M., et al.: Land-Atmosphere Interactions Exacerbated the
506 Drought and Heatwave Over Northern Europe During Summer 2018, *AGU Advances*, 2,
507 e2020AV000283., doi: 10.1029/2020AV000283, 2020.
- 508 Doherty, R. M., Heal, M. R., and O'Connor, F. M.: Climate change impacts on human health over
509 Europe through its effect on air quality, *Environmental Health*, 16(1), 33–44, doi:10.1186/s12940-
510 017-0325-2, 2017.



- 511 Drouard, M., Kornhuber, K. and Woollings, T.: Disentangling Dynamical Contributions to Summer
512 2018 Anomalous Weather Over Europe, *Geophysical Research Letter*, 46, 12537-12546,
513 doi:10.1029/2019GL084601, 2020.
- 514 Emmons, L. K., Arnold, S. R., Monks, S. A., et al.: The POLARCAT Model Intercomparison Project
515 (POLMIP): overview and evaluation with observations, *Atmospheric Chemistry and Physics*, 15, 6721–
516 6744, doi:10.5194/acp-15-6721-2015, 2015.
- 517 Forster, P., Ramaswamy, V., Artaxo, P., et al.: Changes in Atmospheric Constituents and in Radiative
518 Forcing, in: Climate Change 2007: The Physical Science Basis. Contribution of Working Group I to the
519 Fourth Assessment Report of the Intergovernmental Panel on Climate Change, Cambridge University
520 Press, Cambridge, United Kingdom and New York, NY, USA, 2007.
- 521 Gaudel, A., Cooper, O.R., Ancellet, G., et al.: Tropospheric Ozone Assessment Report: Present day
522 distribution and trends of tropospheric ozone relevant to climate and global atmospheric chemistry
523 model evaluation. *Elementa*, 6(39), 1-58, doi:10.1525/elementa.291, 2018.
- 524 Graham, A. M., Pringle, K. J., Pope, R. J., et al.: Impact of the 2019/2020 Australian megafires on air
525 quality and health, *GeoHealth*, 5, e2021GH000454, doi:10.1029/2021GH000454, 2020.
- 526 Granier, C., Bessagnet, B., Bond, T., et al.: Evolution of anthropogenic and biomass burning emissions
527 of air pollutants at global and regional scales during the 1980–2010 period, *Climatic Change*, 109,
528 163-190, doi:10.1007/s10584-011-0154-1, 2011.
- 529 Guerreiro, S.B., Dawson, R.J., Kilsby, C., et al.: Future heat-waves, droughts and floods in 571
530 European cities, *Environmental Research Letters*, 13, 034009, 10.1088/1748-9326, 2018.
- 531 Hollaway, M.J., Arnold, S.R., Challinor, A. J. and Emberson, L.D: Intercontinental trans-boundary
532 contributions to ozone-induced crop yield losses in the North Hemisphere, *Biogeosciences*, 9, 271–
533 2929, doi: 10.5194/bg-9-271-2012, 2012.
- 534 Jacob, D.J., and Winner, D.A.: Effect of climate change on air quality, *Atmospheric Environment*, 43
535 (1), 51-63, doi:10.1016/j.atmosenv.2008.09.051, 2009.
- 536 Jerrett, M., Burnett, R.T., Pope, C.A., et al.: Long-term ozone exposure and mortality, *The New
537 England Journal of Medicine*, 360 (11), 1085–1095, doi: 10.1056/NEJMoa0803894, 2009.
- 538 Kaiser, J.W., Hell, A., Andreae, M.O., et al.: Biomass burning emissions estimated with a global fire
539 assimilation system based on observed fire radiative power, *Biogeosciences*, 9(1), 527–554, doi:
540 10.5194/bg-9-527-2012, 2012.
- 541 Lhotka, O., Kysely, J. and Farda, A.: Climate change scenarios of heat waves in Central Europe and
542 their uncertainties, *Theoretical and Applied Climatology*, 131, 1043-1054, doi: 10.1007/s00704-016-
543 2031-3, 2017.
- 544 Li, M., Yao, Y., Simmonds, I., et al.: Collaborative impact of the NAO and atmospheric blocking on
545 European heat waves, with a focus on the hot summer of 2018, *Environmental Research Letters*, 15,
546 114003, doi:10.1088/1748-9326/aba6ad, 2020.
- 547 Liu, X., He, B., Guo, L., et al.: Similarities and differences in the mechanisms causing the European
548 summer heat waves in 2003, 2010 and 2018, *Earth's Future*, e2019EF001386, doi:
549 10.1029/2019EF001386, 2020.
- 550 Mann, G.W., Carslaw, K.S., Spracklen, D.V., et al.: Description and evaluation of GLOMAP-mode: A
551 modal global aerosol microphysics model for the UKCA composition-climate model. *Geoscientific
552 Model Development*, 3(2), 519–551, doi:10.5194/gmd-3-519-2010, 2010.



- 553 Matsueda, M.: Predictability of Euro-Russian blocking in summer of 2010, *Geophysical Research*
554 *Letters*, 38, L06801, doi:10.1029/2010GL046557, 2011.
- 555 Methven, J., Arnold, S.R., O'Connor, F.M., et al.: Estimating photochemically produced ozone
556 throughout a domain using flight data and a Lagrangian model, *Journal of Geophysical Research:*
557 *Atmospheres*, **10** (D9), doi:10.1029/2002JD002955, 2003.
- 558 Miles, G.M., Siddans, R., Kerridge, B. J., Latter, B. G., and Richards, N. A. D.: Tropospheric ozone and
559 ozone profiles retrieved from GOME-2 and their validation, *Atmospheric Measurement Techniques*,
560 **8**, 385–398, doi:10.5194/amt-8-385-2015, 2015.
- 561 Monks, S.A., Arnold, S.R., Hollaway, M. J., et al.: The TOMCAT global chemistry transport model v1.6:
562 Description of chemical mechanism and model evaluation, *Geoscientific Model Development*, **10** (8),
563 3025–3057, doi:10.5194/gmd-10-3025-2017, 2017.
- 564 Morgenstern, O., Hegglin, M.I., Rozanov, E., et al.: Review of the global models used with phase 1 of
565 the Chemistry-Climate Model Initiative (CCMI), *Geoscientific Model Development*, **10** (2), 639–671,
566 doi:10.5194/gmd-10-639-2017, 2017.
- 567 Munro, R., Siddans, R., Reburn, W. J., and Kerridge, B. J.: Direct measurement of tropospheric ozone
568 distributions from space, *Nature*, **392**, 168–171, doi:10.1038/32392, 1998.
- 569 Pacifico, F., Harrison, S.P., Jones, C.D., et al.: Evaluation of a photosynthesis-based biogenic isoprene
570 emission scheme in JULES and simulation of isoprene emissions under present-day climate
571 conditions, *Atmospheric Chemistry and Physics*, **11**, 4371–4389, doi:10.5194/acp-11-4371-2011,
572 2011.
- 573 Palmer, P., I., Marvin, M., R., Siddans, R., et al.: Nocturnal survival of isoprene linked to formation
574 of upper tropospheric organic aerosol, *Science*, **375** (6580), 562–566,
575 doi:10.1126/science.abg4506.
- 576 PHE (Public Health England), PHE heatwave mortality monitoring, available at:
577 [https://assets.publishing.service.gov.uk/government/uploads/system/uploads/attachment_data/file](https://assets.publishing.service.gov.uk/government/uploads/system/uploads/attachment_data/file/942648/PHE_heatwave_report_2018.pdf)
578 [/942648/PHE_heatwave_report_2018.pdf](https://assets.publishing.service.gov.uk/government/uploads/system/uploads/attachment_data/file/942648/PHE_heatwave_report_2018.pdf) (last accessed 3rd February 2022), 2019.
- 579 Pirovano, G., Balzarini, A., Bessagnet, B., et al.: Investigating impacts of chemistry and transport
580 model formulation on model performance at European scale, *Atmospheric Environment*, **53**, 93–109,
581 doi:10.1016/j.atmosenv.2011.12.052, 2012.
- 582 Pope, R.J., Savage, N.H., Chipperfield, M.P., et al.: The influence of synoptic weather regimes on UK
583 air quality: analysis of satellite column NO₂, *Atmospheric Science Letters*, **15**, 211– 217,
584 doi:10.1002/asl22.492, 2014.
- 585 Pope, R.J., Butt, E.W., Chipperfield, M.P., et al.: The impact of synoptic weather on UK surface ozone
586 and implications for premature mortality. *Environmental Research Letters*, **11**, 124004,
587 doi:10.1088/1748-9326/11/12/124004, 2016.
- 588 Pope, R.J., Arnold, S.R., Chipperfield, M.P., et al.: Substantial Increases in Eastern Amazon and
589 Cerrado Biomass Burning-Sourced Tropospheric Ozone. *Geophysical Research Letters*, **47** (3),
590 e2019GL084143, doi:10.1029/2019GL084143, 2020.
- 591 Pope, R. J., Kerridge, B. J., Siddans, R., et al.: Large enhancements in southern hemisphere satellite-
592 observed trace gases due to the 2019/2020 Australian wildfires, *Journal of Geophysical Research:*
593 *Atmospheres*, 1–13, doi:10.1029/2021jd034892, 2021.



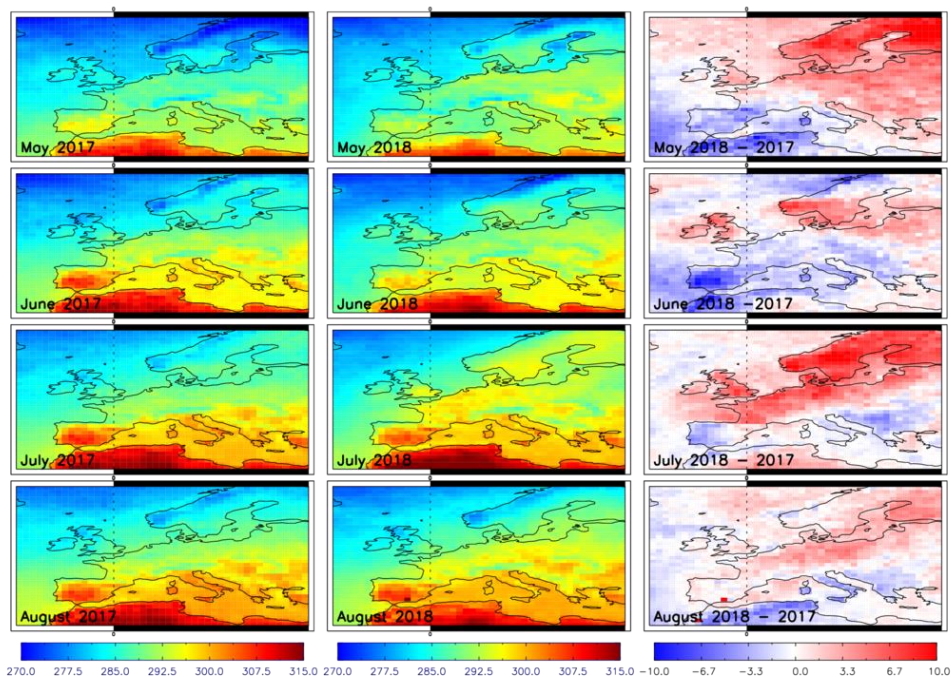
- 594 Pyrgou, A., Hadjinicolaou, P and Santamouris, M: Enhanced near-surface ozone under heatwave
595 conditions in a Mediterranean island, *Scientific Reports*, 8, 9191, doi:10.1038/s41598-018-27590-z,
596 2018.
- 597 RAL Space, Optimal Estimation Method retrievals with IASI, AMSU and MHS – Final Report Version
598 5.2, available at: http://cedadocs.ceda.ac.uk/1377/1/iasi_mhs_final_report_v5p2.pdf (last accessed
599 17/08/2020), 2015.
- 600 Rebetez, M., Dupont, O. and Giroud, M.: An analysis of July 2006 heatwave extent in Europe
601 compared to the record year of 2003, *Theoretical and Applied Climatology*, 95, 1-7,
602 doi:10.1007/s00704-007-0370-9, 2008.
- 603 Richards, N.A.D, Arnold, S.R., Chipperfield, M.P., et al.: The Mediterranean summertime ozone
604 maximum: global emission sensitivities and radiative impacts, *Atmospheric Chemistry and Physics*,
605 13, 2231-2345, doi:10.5194/acp-13-2331-2013, 2013.
- 606 Riese, M., Ploeger, F., Rap, A., et al.: Impacts of uncertainties in atmospheric mixing on simulated
607 UTLS composition and related radiative effects, *Journal of Geophysical Research: Atmospheres*, 117,
608 D16305, doi:10.1029/2012jd017751, 2012.
- 609 Rodgers, C.D.: Inverse methods for atmospheric sounding: Theory and practice. New Jersey, USA:
610 World Science. 2000.
- 611 Scott, P.A., Stone, D.A. and Allen, M.R.: Human contributions to the European heatwave of 2003,
612 *Nature*, 432, 610-614, doi:10.1038/nature03089, 2004.
- 613 Sitch, S., Cox, P.M., Collins, W.J., & Huntingford, C.: Indirect radiative forcing of climate change
614 through ozone effects on the land carbon sink, *Nature*, 448, 791–795, doi:10.1038/nature06059,
615 2007.
- 616 Smith, N.E., Kooijmans, L.M.J., Koren, G., et al.: Spring enhancements and summer reduction in
617 carbon uptake during the 2018 drought in Northwestern Europe, *Philosophical Transactions B*, 375,
618 20190509, doi:10.1098/rstb.2019.0509, 2020.
- 619 Thomas, M.A. and Devasthale, A.: Sensitivity of free tropospheric carbon monoxide to atmospheric
620 weather states and their persistency: an observational assessment over the Nordic countries,
621 *Atmospheric Chemistry and Physics*, 14, 11545–11555, doi:10.5194/acp14-11545-2014, 2014.
- 622 Van Dingenen, R., Dentener, F.J., Raes, F., et al.: The global impact of ozone on agriculture crop
623 yields under current and future air quality legislation. *Atmospheric Environment*, 43(3), 604–618,
624 doi:10.1016/j.atmosenv.2008.10.033, 2009.
- 625 Vieno, M., Dore, A.J., Stevenson, D.S., et al.: Modelling surface ozone during the 2003 heat-wave in
626 the UK, *Atmospheric Chemistry and Physics*, 10, 7963-7978, doi:10.5194/acp-10-7963-2010, 2010.
- 627 WHO (World Health Organisation), Ambient (outdoor) air pollution, available at:
628 [https://www.who.int/news-room/fact-sheets/detail/ambient-\(outdoor\)-air-quality-and-health](https://www.who.int/news-room/fact-sheets/detail/ambient-(outdoor)-air-quality-and-health) (last
629 accessed 3rd February 2022), 2021.
- 630
- 631
- 632
- 633



634

635

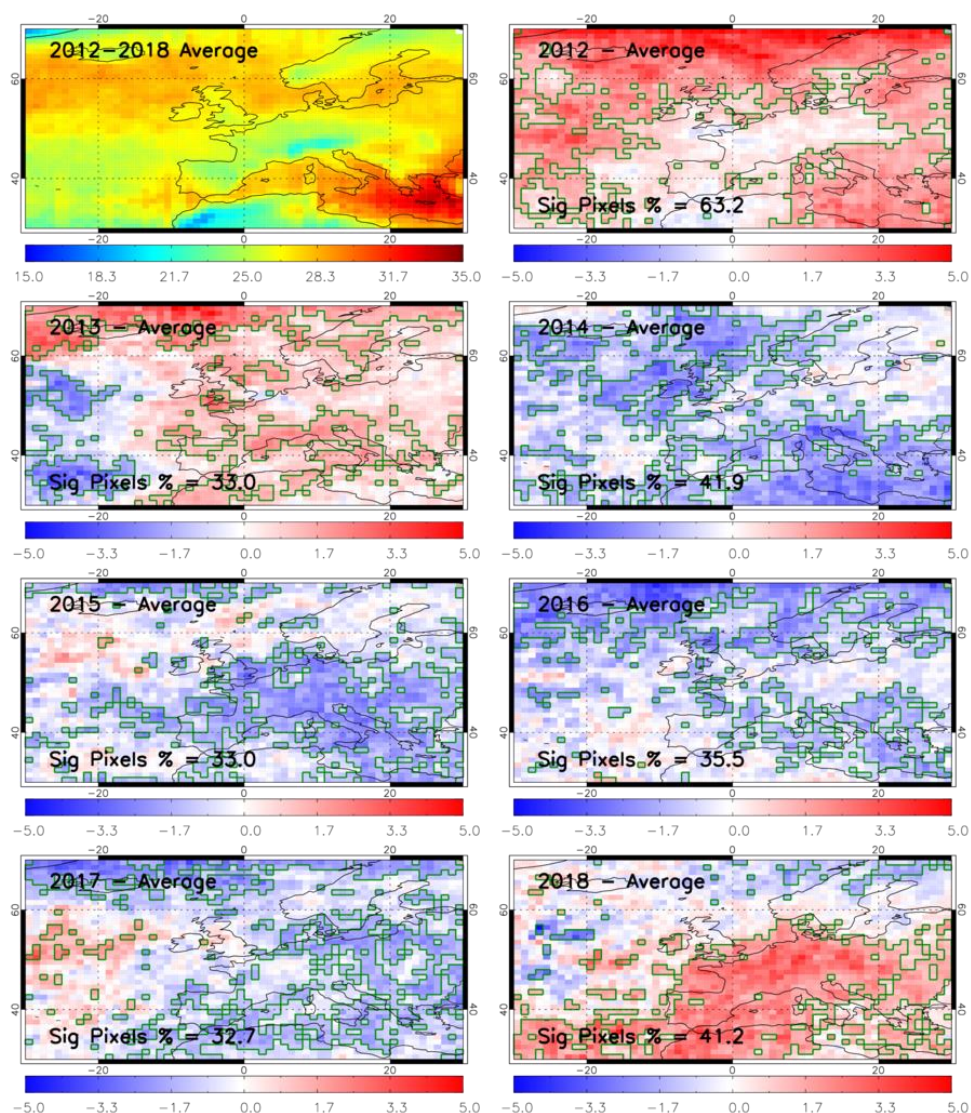
636 **Figures:**



637

638 **Figure 1:** Surface temperature (K) over Europe for May to August in 2017 (LHS), 2018 (middle) and
639 2018-2017 difference (RHS) retrieved from MetOp-A IASI, MHS and AMSU by the IMS scheme.

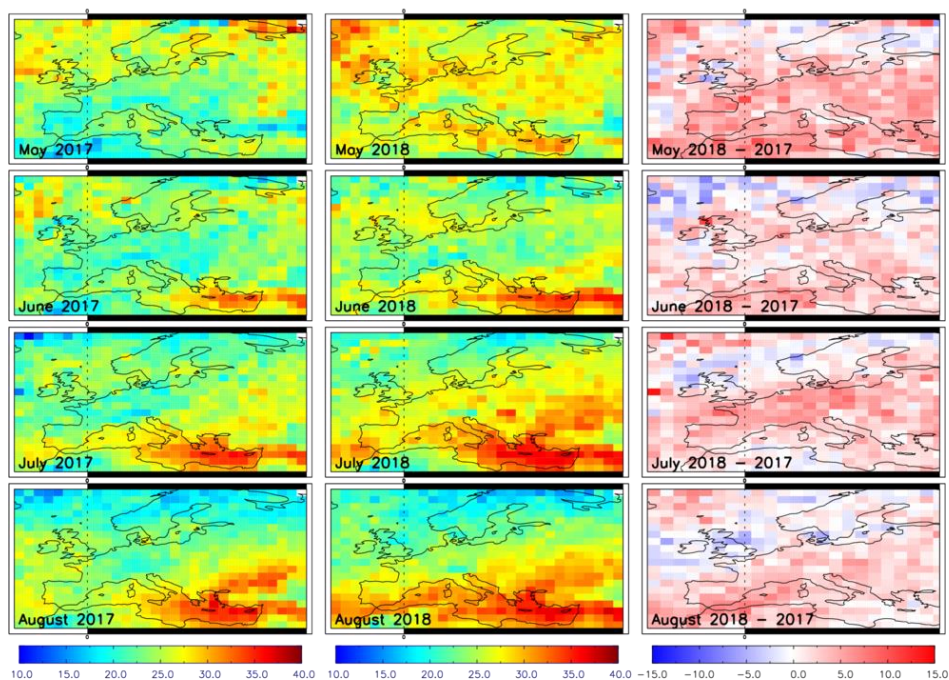
640



641

642 **Figure 2:** Sub-column ozone (SCO_3 , surface-450 hPa), in Dobson units (DU), retrieved from GOME-2
643 on Metop-A averaged across May to August between 2012 and 2018 (top left panel) and the
644 corresponding difference from the 2012-18 mean for each year, respectively. The green-polygon-
645 outlined regions show where the year-specific seasonal average is significantly different (95%
646 confidence level based on the Wilcoxon Rank Test (WRT)) from the long-term (2012-2018) seasonal
647 average. The “Sig Pixel %” label indicates the number of pixels in the domain with significant
648 differences.

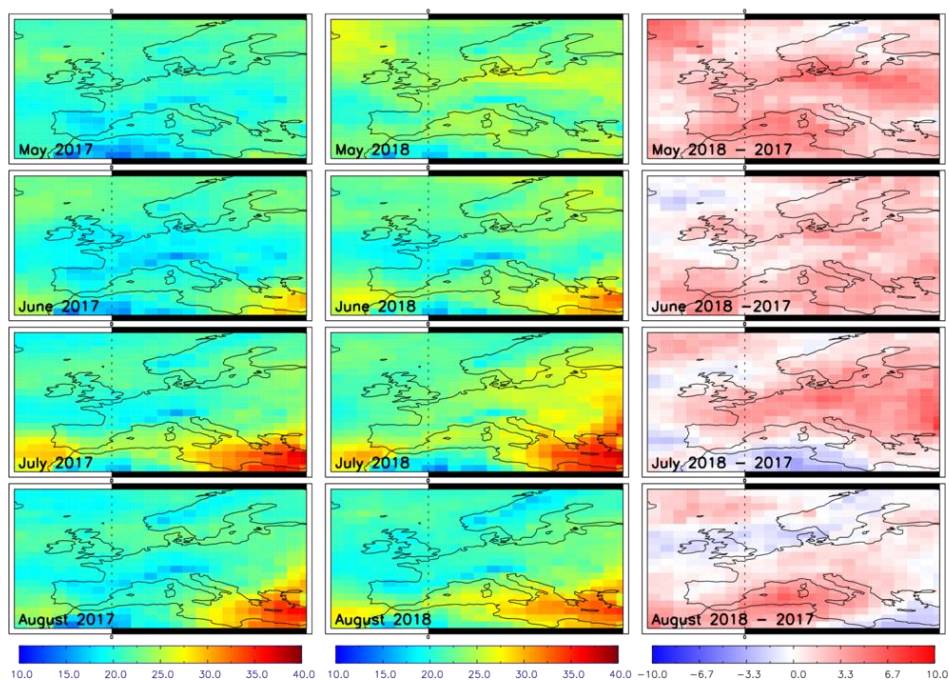
649



650

651 **Figure 3:** SCO_3 (DU) from GOME-2 over Europe for May to August in (left column) 2017, (middle
652 column) 2018 and (right column) 2018-2017 difference.

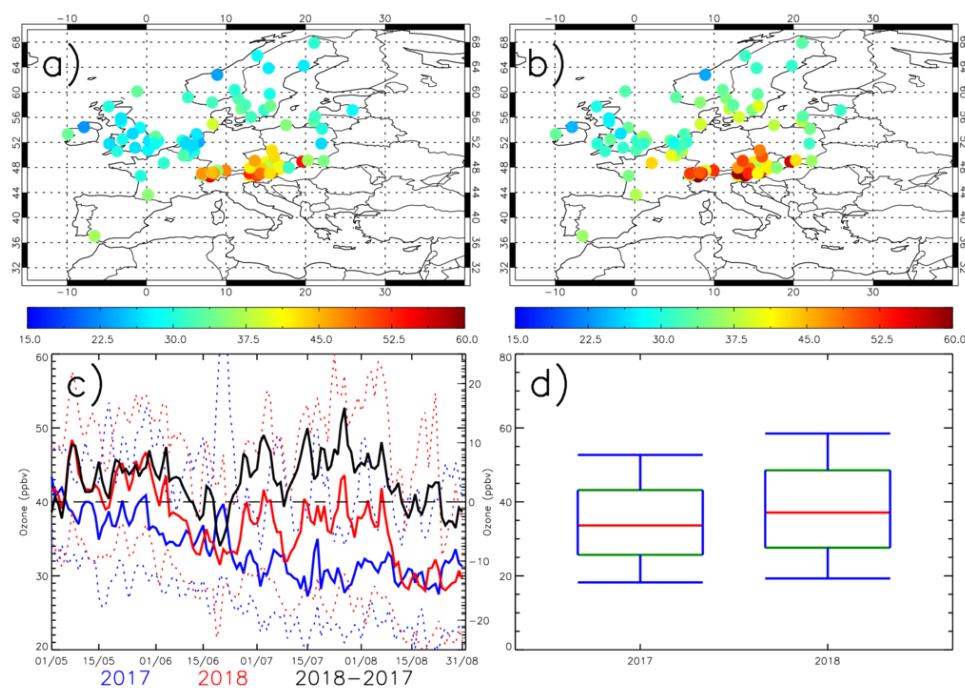
653



654

655 **Figure 4:** CO_2 (DU) for May to August in 2017 (LHS), 2018 (middle) and 2018-2017 difference (RHS)
656 over Europe retrieved from MetOp-A IASI, MHS and AMSU by the IMS scheme.

657



658

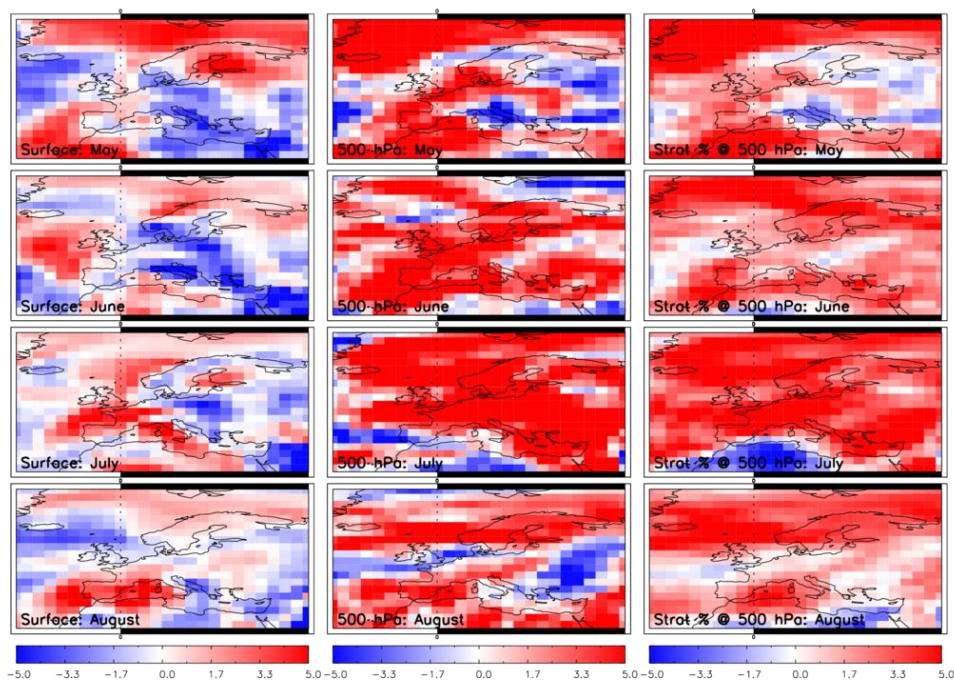
659 **Figure 5:** European surface ozone (ppbv) for a) May-June-July-August (MJA) 2017, b) MJA 2018), c)

660 regional time series for MJA 2017 (blue), MJA 2018 (red) and the 2018-2017 difference (black) and

661 d) box-whisker plots for MJA 2017 and 2018. In panel d) the median, 25th & 75th percentiles and

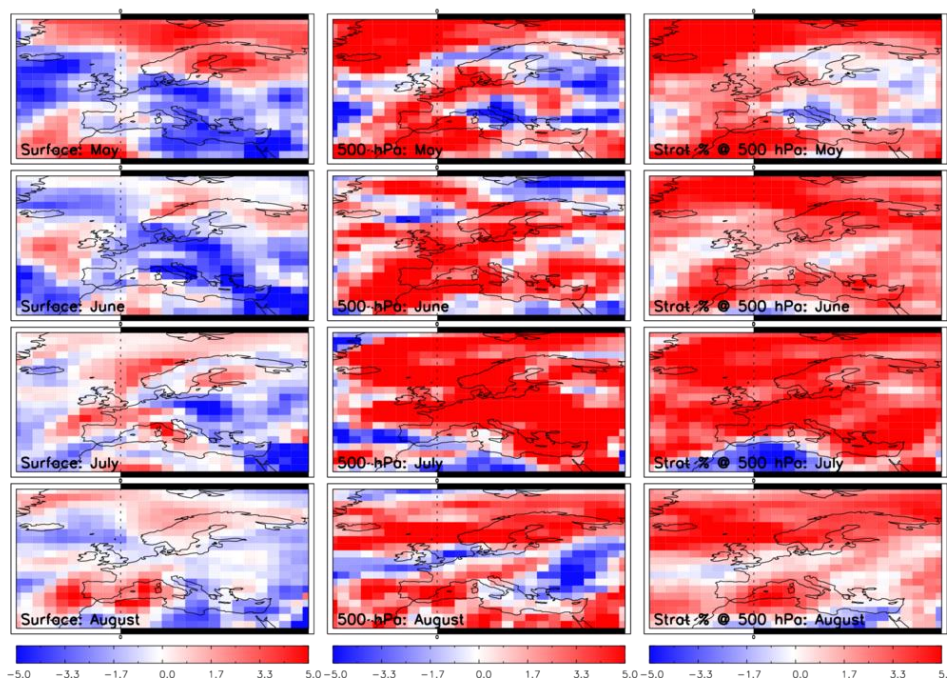
662 10th & 90th percentiles are shown by the red, green and blue lines, respectively.

663



664
665
666
667

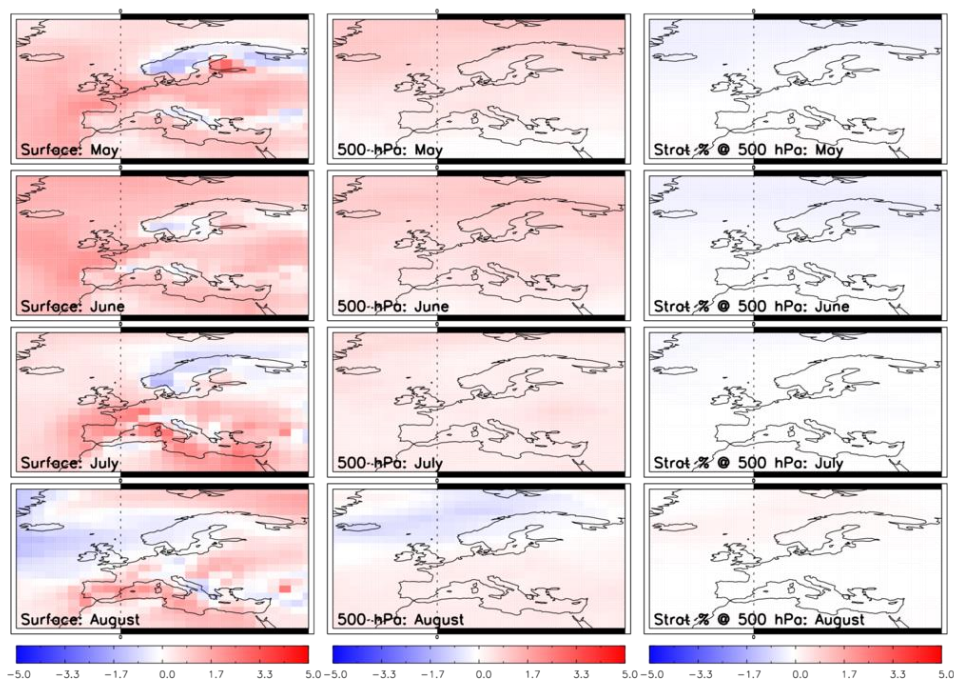
Figure 6: TOMCAT ozone (ppbv) 2018-2017 differences for May to August for the surface (LHS), 500 hPa (middle) and the stratospheric contribution (%) to the 500 hPa layer (RHS).



668

669 **Figure 7:** TOMCAT ozone (ppbv) 2018-2017 differences for May to August for the fixed emissions
670 simulation (Fixed_EMIS) for the surface (LHS), 500 hPa (middle) and the stratospheric contribution
671 (%) to the 500 hPa layer (RHS).

672



673

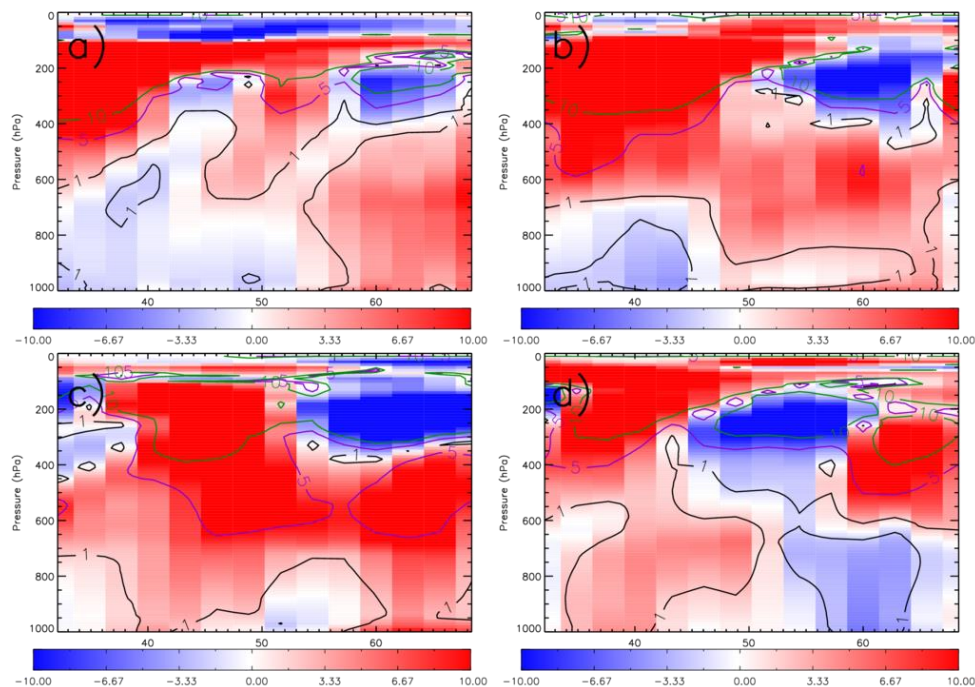
674 **Figure 8:** TOMCAT ozone (ppbv) 2018-2017 differences for May to August for the fixed meteorology
675 simulation (Fixed_MET) for the surface (LHS), 500 hPa (middle) and the stratospheric contribution (%)
676 to the 500 hPa layer (RHS).

677

678

679

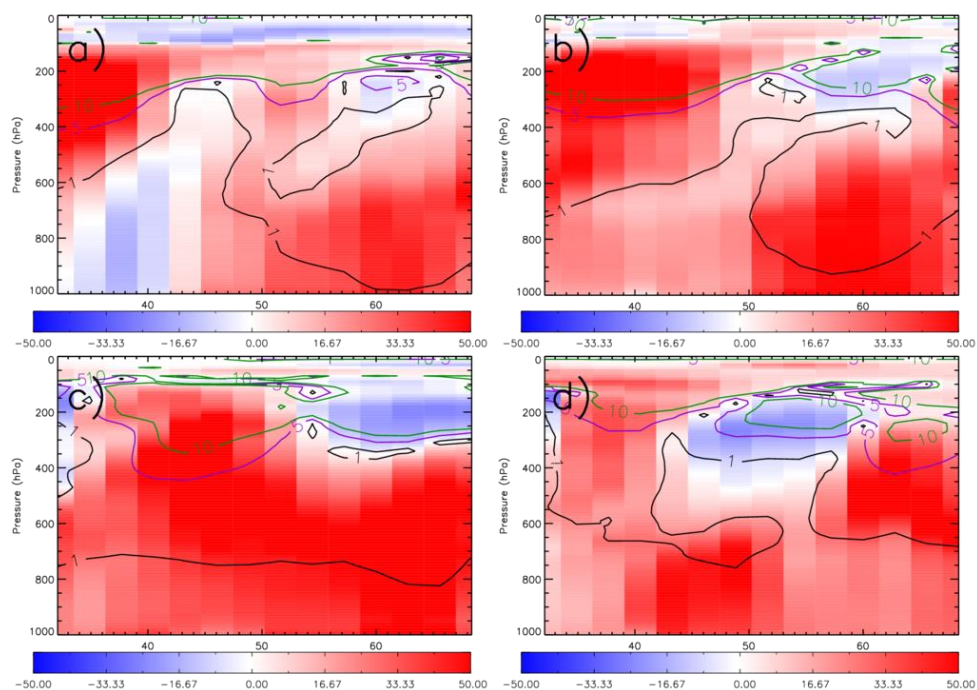
680



681

682 **Figure 9:** TOMCAT ozone, zonally averaged between 20°W and 40°E, 2018-2017 percentage
683 differences (absolute difference (ppbv) shown as solid lines) from the control simulation. Panels a)-d)
684 represent the monthly averages for May, June, July and August.

685



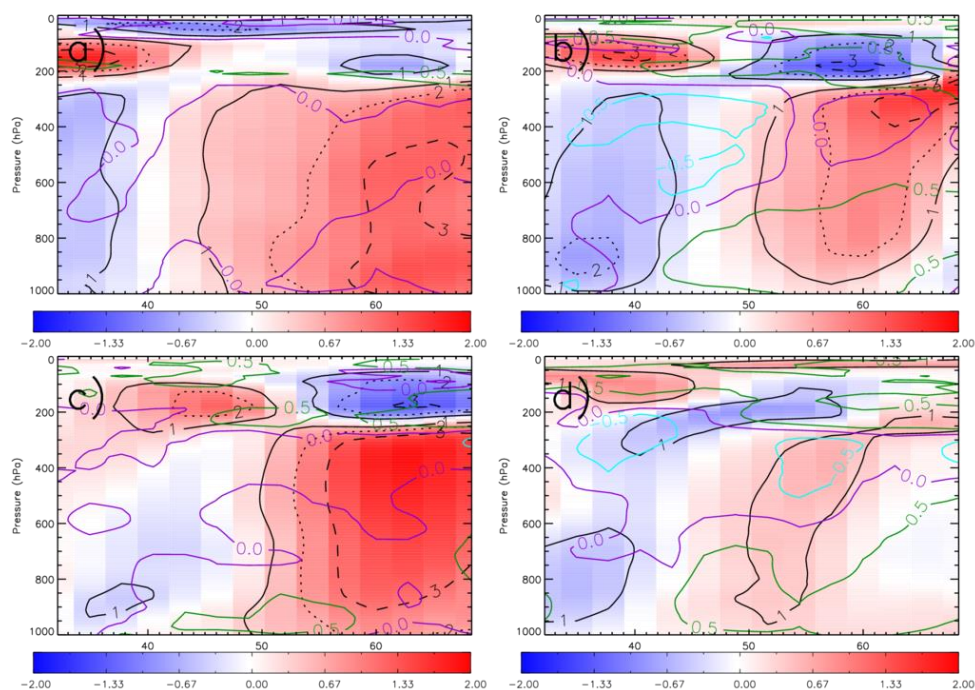
686

687 **Figure 10:** TOMCAT stratospheric ozone tracer, zonally averaged between 20°W and 40°E, 2018-2017
688 percentage differences (absolute difference (ppbv) shown as solid lines) from the control simulation.
689 Panels a-d) represent the monthly averages for May, June, July and August.

690

691

692



693

694 **Figure 11:** TOMCAT temperature, zonally averaged between 20°W and 40°E, 2018-2017 percentage
695 differences (absolute difference (K) shown by black solid, dotted and dashed lines) from the control
696 simulation. Overplotted are contours of the temporal correlation (i.e. within each grid box) between
697 the temperature and ozone 2018-2017 differences. Panels a)-d) represent the monthly averages for
698 May, June, July and August.

699

700

701

702

703

704

705

706

707

708

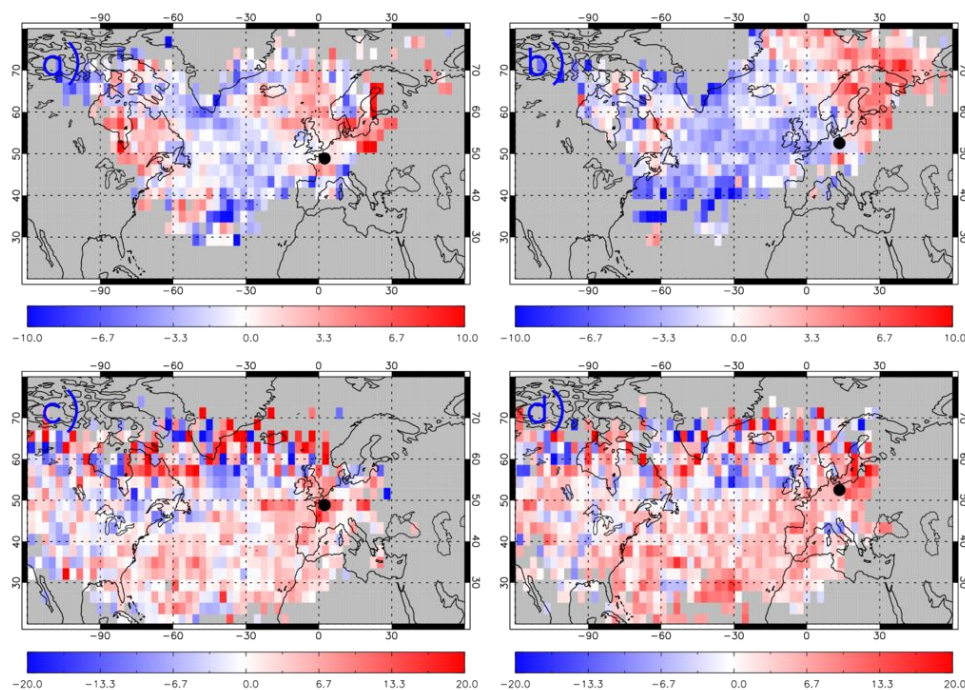
709

710

711



712



713

714 **Figure 12:** The difference between May-August 2018 and May-August 2017 (i.e. 2018-2017) ROTRAJ
715 back-trajectories (10 days), weighted by the average TOMCAT O₃ (ppbv) concentration along each
716 trajectory path, gridded onto the TOMCAT horizontal resolution for a) Paris at the surface, b) Berlin
717 at the surface, c) Paris at approximately 500 hPa and d) Berlin at approximately 500 hPa. The black
718 circles represent the location of Paris or Berlin, where the trajectories were released from.

719